International Journal of Fatigue, Volume 54

International Journal of Fatigue 54 (2013) 106–117

Contents lists available at SciVerse ScienceDirect

International Journal of Fatigue

journal homepage: www.elsevier.com/locate/ijfatigue

Evaluating surface deformation and near surface strain hardening resulting from shot peening a tempered martensitic steel and application to low cycle fatigue

K.A. Soady [a,b,*], B.G. Mellor [a], G.D. West [c], G. Harrison [d], A. Morris [b], P.A.S. Reed [a]

[a] Materials Research Group, Faculty of Engineering and the Environment, University of Southampton, Highfield, Southampton SO17 1BJ, UK
[b] E.ON New Build & Technology Ltd., Ratcliffe on Soar, Nottingham NG11 0EE, UK
[c] Department of Materials, Loughborough University, Leicestershire LE11 3TU, UK
[d] Materials Science Centre, University of Manchester, Oxford Road, Manchester M13 9PL, UK

ARTICLE INFO

Article history:
Received 18 December 2012
Received in revised form 20 March 2013
Accepted 22 March 2013
Available online 6 April 2013

Keywords:
Plastic deformation
Shot peening
Low cycle fatigue
X-ray diffraction
Electron backscatter diffraction

ABSTRACT

The plastic deformation resulting from shot peening treatments applied to the ferritic heat resistant steel FV448 has been investigated. Two important effects have been quantified: surface roughness and strain hardening. 2D and 3D tactile and optical techniques for determining surface roughness amplitude parameters have been investigated; it was found that whilst R_a and S_a were consistent, S_z was generally higher than R_z due to the increased probability of finding the worst case surface feature. Three different methods for evaluating the plastic strain profile have been evaluated with a view to establishing the variation in yield strength near the surface of a shot peened component. Microhardness, X-ray diffraction (XRD) line broadening and electron backscatter diffraction (EBSD) local misorientation techniques were applied to both uniaxially deformed calibration samples of known plastic strain and samples shot peened at intensities varying from 4A to 18A to establish the variation in plastic strain and hence the variation in yield strength. The results from the three methods were compared; XRD and EBSD profiles were found to be the most similar with microhardness profiles extending much deeper into the sample. Changes in the measured plastic strain profile after exposure to low cycle fatigue and the correlation of these changes with the cyclic stress–strain behaviour of the material are also discussed with a view to assessing the importance of the dislocation profile in component life assessment procedures.

1. Introduction

Shot peening is a cold work process typically applied to components to improve fatigue resistance in critical areas. Stress concentrating regions are bombarded with high velocity shot of a hard material. This results in plastic deformation at the surface of the component, characterised by a dimpled topography and near surface strain hardening, thus increasing the local yield strength of the material. Compressive residual stresses are also formed as a result of the misfit strain between the plastically deformed surface and the elastically deformed sub-surface layers. Whilst this process has been applied for many years, current interest is focussed on including the effects of the shot peening process in component remnant life models rather than simply using the process to add extra conservatism to the model.

One example application is to shot peened industrial low pressure steam turbine blade to disc interfaces. Non-destructive testing is typically carried out every 12 years and damage tolerant life assessment modelling is performed based on the worst case defects to underwrite service for the next period or to define a repair and replacement schedule. The development of life assessment methods with the potential to defer invasive inspections, improve the reliability of repair and replacement schedules and extend component life are of significant interest in the power generation industry where the loss during a typical outage of 8–12 weeks on a 500 MW unit is >£M.

Inclusion of shot peening effects in remnant fatigue life modelling requires detailed consideration of the inter-relationship between surface roughness and strain hardening on initiation characteristics (surface roughness tends to accelerate initiation, whereas strain hardening tends to retard initiation) and residual and applied stresses (as influenced by near surface strain hardening) on crack propagation (compressive residual stresses tend to reduce damaging tensile applied mean stresses). In some cases, there may also be the additional complication of phase transforma-

* Corresponding author at: Materials Research Group, Faculty of Engineering and the Environment, University of Southampton, Highfield, Southampton SO17 1BJ, UK. Tel.: +44 (0) 2476 192010.
E-mail address: K.A.Soady@soton.ac.uk (K.A. Soady).

0142-1123/$ - see front matter © 2013 Elsevier Ltd. All rights reserved.
http://dx.doi.org/10.1016/j.ijfatigue.2013.03.019

tions induced near the peened surface which may also affect the near surface material properties, or cyclic hardening or softening of the near surface material as a result of the accumulation of plastic strain (depending on the specific properties of the material in question). Furthermore, the residual stress and strain hardening profiles may be modified by the application of service temperature and load spectrums; these modifications are heavily dependent on the behaviour of the material in question under cyclic load. These relationships are complex and are dealt with in significantly more detail in a recent review by one of the present authors [1]. There is thus a clear requirement for well-defined procedures for determining the residual stress profile, surface deformation, or roughness and near surface strain hardening resulting from any given shot peening system.

Methods for determining residual stress profiles by X-ray diffraction (XRD) [2] and hole drilling [3] are well established, with both methods able to measure near surface compressive residual stresses in shot peened components [4]. Hence the focus in the present paper is on establishing the most appropriate methods for characterising surface roughness features and near surface strain hardening with a view to their inclusion in life assessment procedures for components operating in the low cycle fatigue (LCF) regime. The manner by which the effects can be included is not described in detail in the present paper; for further information, the reader is directed to a recent review by some of the present authors [5].

Many parameters can be defined to describe surface roughness; despite some indications that describing other parameters such as R_t (which can capture worst case defect data) and R_{sk} and R_{ku} (which can capture more statistical information about the surface profile) [6], R_a remains the parameter of choice in the majority of papers considering shot peeing surface roughness effects (see for example [7]), although some more recent works now report areal parameters (see for example [8]). Whilst detrimental surface roughness effects are often considered to be insignificant in systems with $2.5 < R_a < 5$ μm, which are dominated by residual stress and strain hardening [9], if the life assessment procedure explicitly accounts for residual stresses and strain hardening, it would be prudent to also consider the effects of surface roughness, possibly by taking account of the stress concentration factor K_t, calculated using the empirical approach of Li et al. [10]. This is particularly important in operating conditions where significant stress relief and changes to the dislocation profile resulting from shot peening occur (as a result of operating temperature and applied stress distributions) [11,12], since surface roughness may become a more dominant factor in assessing fatigue life. For example, in stress relieved AISI 4140, even a surface roughness of $R_a < 1.4$ μm ($R_t < 14$ - μm) had a detrimental effect compared to polished samples of $R_a = 0.3$ μm ($R_t < 5$ μm) [13].

Recently there has been a drive towards three dimensional topographical characterisation of surfaces with new standards defining area parameters such as S_a and S_t [14] and the tactile and optical methods which can be used to characterise them [15]. In a recent study, Child et al. [8] used white-light interferometry to determine the S_a resulting from shot peening, although the relationship between the areal parameters and linear parameters was not confirmed. This relationship may be critical if such measurements are to be used in determining roughness induced stress concentration factors and thus included in component life assessment procedures.

The strain hardening profile resulting from shot peening can be characterised (see for example [8,11,12,16–19]). Any changes to the dislocation distribution during LCF should also be considered since this rearrangement is strongly related to the relaxation of residual stresses and can help identify locations where initiation is likely [11,12,20]. There are three well recognised methods for determining the extent of cumulative plastic strain, namely microhardness, XRD line broadening (typically measured using full width at half maximum (FWHM) data) and electron backscatter diffraction (EBSD) misorientation analyses.

For shot peened components, these plastic strain measures are commonly quoted 'as is' and not converted to a plastic strain magnitude (see for example uncalibrated hardness [16], laboratory XRD FWHM [12] and EBSD [8]); this conversion is essential if the varying yield strength near the surface of a shot peened component is to be considered in life assessment.

The relationship between microhardness and yield strength has been presented in several papers; the causal link between the two parameters is clear: strain hardening and the associated increase in dislocation density increases the resistance to plastic deformation. However, the mathematical nature of the relationship is not well defined. Cahoon et al. [21] related hardness to yield strength using the strain hardening exponent whilst Fontanari et al. [4] suggest that the ratio of elevated yield strength to bulk yield strength in aluminium alloys is the same as the measured hardness ratio. In power law hardening materials perhaps the most physically representative model is that used by Srikant et al. [22] relating hardness to plastic strain using a power law.

Neglecting instrumental effects, diffraction peaks can be broadened by reductions in crystallite size and the presence of microstrains. For diffraction profiles that are known with high statistical significance, complex deconvolution analyses can be used to separate the crystallite size and strain effects [23]; these techniques are now often implemented in commercial diffraction peak analysis software, such as TOPAS [24]. The Williamson–Hall approach can also be used to separate size and strain effects and has been demonstrated for shot peened samples by Tan et al. [25]. However, the laboratory XRD systems used to investigate shot peened materials (typically for residual stresses) are often not optimised for such complex analyses and deconvolution is not possible. In this case, when relative values will suffice, the calibration approach described by Prevéy for nickel based alloys can be applied [17,26]. Peak width was related to plastic strain by an exponential relationship; the plastic strain can then be used to determine the variation of yield strength as a function of depth [26].

EBSD techniques have recently been growing in popularity for measuring plastic strain. Geometrically necessary dislocations resulting from crystallographic slip result in crystal orientation changes within the material which can be detected [27]. This affects both the quality of the diffraction patterns and the local orientation. Early work quantified the 'diffuseness' of the Kikuchi line pairs using the gradient of the pixel grey level on traversing the line [28].

More recently, image quality parameters have been used qualitatively (since they are influenced by other effects such as interaction volume, sample surface and sample tilt [27]), with quantitative methods focussing on crystallographic misorientation parameters. This is often quantified as the spread in crystallographic orientation within a grain. Linear relationships between misorientation and plastic strain have been shown in both austenitic stainless steel and nickel alloys [27]. Local misorientation methods have also been employed in 304L stainless steel and nickel alloy 690 [29] and also show a linear relationship. Given possible saturation effects [29], it is crucial to extend the calibration beyond the maximum of 20% reported in these studies if the method is to be extended to analysing the plastic strain distribution resulting from shot peening where strains are typically in excess of 20% and in the extreme may reach 50% [17].

It was upon comparison of the indicated plastic strain distributions resulting from each measurement technique that we realised a systematic comparison was required. Table 1 details the plastic

Table 1
Comparison of indicated plastic strain depths resulting from shot peening (6–8A) Udimet 720Li.

Method	Depth (μm)	Source
Microhardness	120	Kim et al. [12]
Laboratory XRD FWHM	100	Kim et al. [12]
Microhardness	100	Child et al. [8]
EBSD grain based misorientation	70	Child et al. [8]

strain measured in shot peened (6–8A) Udimet 720Li by two different research groups using different methods. The results from the microhardness technique show reasonable repeatability; the indicated depth by the XRD technique is somewhat reduced whilst the depth measured by the EBSD technique is around half that measured by the microhardness technique.

The objective of this paper is twofold. To the best of the authors' knowledge, there has not been an explicit comparison of two dimensional and three dimensional surface roughness characterisation techniques or of calibrated microhardness, laboratory XRD and EBSD methods for evaluating plastic strain distribution. Before these measurements can be accepted into industrial component lifing procedures for shot peened components, the methods must be systematically evaluated and standards adopted; the comparisons of the methods in this paper are a first step in this process. The second objective of the paper is to apply the plastic strain characterisation methods first in evaluating the plastic strain resulting from varying shot peening processes and second to consider the manner in which the corresponding dislocation distributions change when subjected to LCF, drawing comparisons with previously published residual stress relaxation data [7] and the cyclic stress–strain behaviour of the material.

2. Material characterisation

The material used throughout this investigation was FV448, a tempered martensitic steel of composition shown in Table 2, typically austenitised at 1150 °C, oil quenched, and then tempered at 650 °C with microstructure shown in Fig. 1. The monotonic Ramberg–Osgood parameters for this material determined under tension in accordance with BS EN 1002-1:2001 [30] at an extension rate of 0.3 mm min^{-1} are $A = 1152$ MPa and $n_m = 0.0587$ [7]. The ambient cyclic stress strain characteristics of the material were also established at three strain ranges ($\Delta\varepsilon = 0.0080$, 0.0110, 0.0155). Tests were in accordance with BS 7270:2006 [31] and the recommendations provided by Hales et al. [32]; the geometry of the cylindrical samples used is illustrated in Fig. 2. Fatigue testing was carried out using a triangular waveform at strain ratio $R_\varepsilon = 0$ and a strain rate of 3×10^{-3} s^{-1}. Strain was controlled using a 12.5 mm gauge length extensometer; load and strain data were both recorded at a frequency such that a minimum of 500 data points were recorded per cycle. The resulting development of peak stresses through life is shown in Fig. 3.

Fig. 3 shows clear cyclic softening through life at all strain ranges investigated. Initially this softening is very rapid before slowing to a relatively constant through life rate; this trend has also been reported elsewhere for other similar 9–12 Cr steels and is a result of rearrangement in the post-quench dislocation structure resulting in a reduction in dislocation density and the conversion of the original fine lath structure to a coarser cellular structure in which the dislocation density at cell walls is higher than that in the cell interior [33,34].

Table 2
Composition of FV448 in wt.% [7].

Element	C	Mn	Si	Ni	Cr	Mo	V	Nb	Fe
Spectrographic analysis	0.12	0.94	0.31	0.74	11.0	0.58	0.31	0.34	Bal

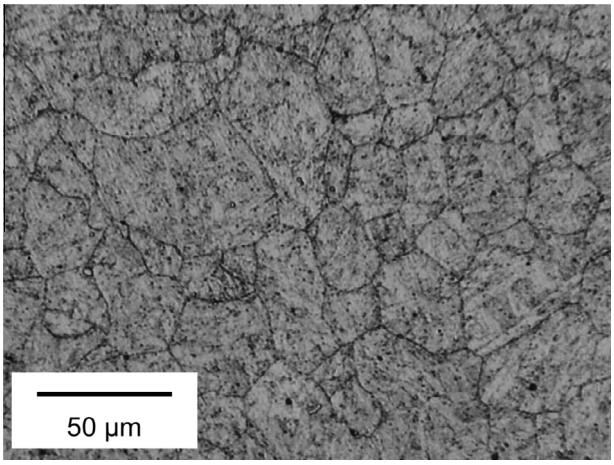

Fig. 1. Optical micrograph of polished and etched (Vilella's Reagent) FV448 illustrating the tempered martensitic microstructure.

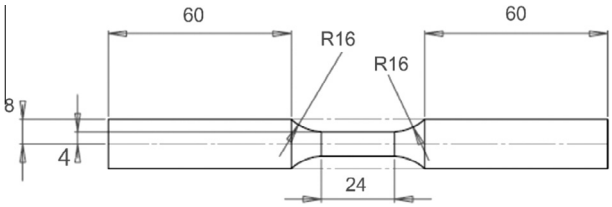

Fig. 2. Cyclic stress strain test sample dimensions in mm.

The three data points obtained (one at each strain range) were used to scale the Ramberg–Osgood relationship for cyclically stabilised behaviour. Stabilisation was assumed to have occurred once the peak stress in a cycle was within 2% of the peak stress at the end of life; the average life fraction at which this condition was met was $0.49N_f$. The monotonic n_m was held constant and A was scaled to minimise the error; the resulting change in A was a drop of 10.6%.

A combined isotropic and non-linear kinematic hardening model [35] was also developed for each strain range. The model was optimised for through life behaviour and the first experimental cycle was not considered due to anomalous behaviour in the first tensile half cycle, after which the kinematic coefficients appeared to change. The modelled through life peak stresses are compared with the experimental data and the results of the cyclically stabilised model in Table 3, assuming that the maximum and minimum stresses predicted by the cyclically stabilised model are the same in each cycle throughout life.

The average error in peak stress resulting from the combined model is less than 1.5%. When comparing the average error, the cyclically stabilised model also appears to perform reasonably well with the highest average absolute error per cycle only 5.1%. However, it is in the maximum absolute error in a half cycle that the combined model performs much better than the cyclically stabilised model; the maximum error in the combined model is 7.6% whereas for the stabilised model it is 13.3%. For both models, the highest error always occurs in the first cycle. However, the error for the combined model is typically reduced to <2.5% by the second cycle ($\Delta\varepsilon = 0.0110$ excluded, it takes 40 cycles at this strain range), whereas for the stabilised model the error is much higher to begin with and reduces more slowly. This results in a greater standard deviation in the error for the stabilised model.

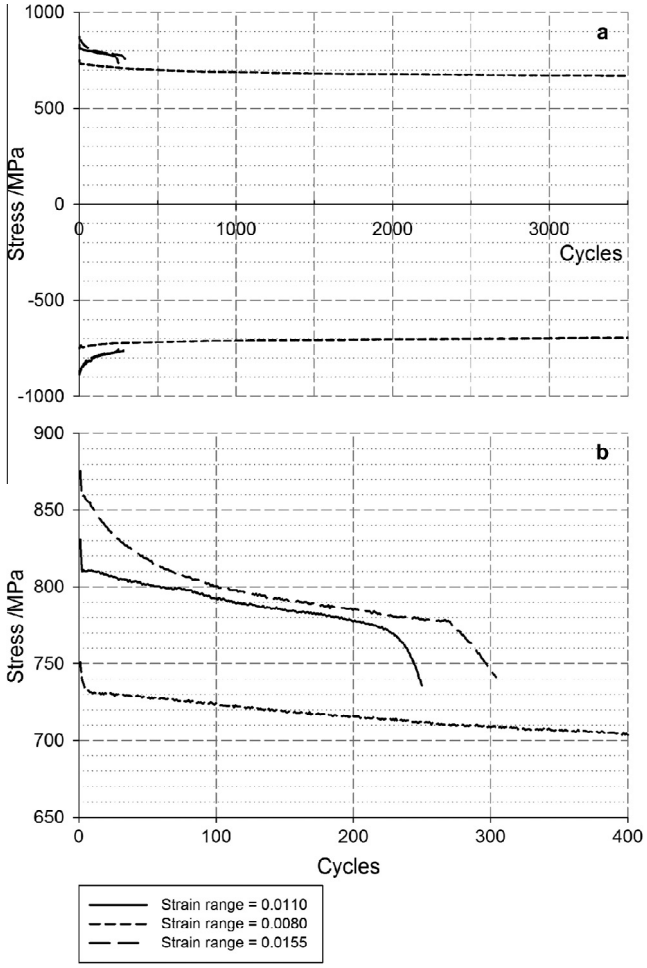

Fig. 3. Development of peak stresses through life at $\Delta\varepsilon = 0.0080$, 0.0110, 0.0155, $R_\varepsilon = -1$ showing (a) through life behaviour and (b) tensile behaviour at the start of life.

Table 3
Statistical comparison of combined and stabilised model peak stresses against experimental data for $\Delta\varepsilon = 0.0080$, 0.0110, 0.0155, $R_\varepsilon = -1$.

Strain range	Model	Average absolute error per half cycle (%)	Standard deviation error per half cycle (%)	Maximum absolute error in an half cycle (%)
0.008	Combined	1.0	0.64	5.4
	Stabilised	2.2	1.36	6.4
0.0110	Combined	1.4	1.66	7.6
	Stabilised	5.1	2.41	13.3
0.0155	Combined	1.3	0.74	6.2
	Stabilised	2.2	2.00	10.4

3. Post shot peen surface roughness and plastic strain measurement methodology

3.1. Sample preparation

Shot peened samples were prepared by Metal Improvement Company, Derby Division according to the four processes outlined in Table 4 (the processes were specified according to shot hardness, diameter, Almen Intensity and coverage; the velocity is shown as an indication of the velocity required to achieve the given Almen Intensity calculated using Metal Improvement Company's in-house Peenstress® software [36]). The results were compared against samples which met the industrial machined component and peen specification of $R_a < 0.8$ μm. Both a Taylor Hobson Form Talysurf 120L stylus profilometer and an Alicona Infinite Focus optical (focus variation) profilometer were used to determine surface roughness average parameters (R_a and S_a) and peak to valley heights (R_z and S_z) [14,37] for each surface condition. To ensure comparability between results, both tactile and optical profile lengths and filters were selected according to BS ISO 4288:1996 [38]; filters for optical areal data were set in accordance with best practice guidelines ensuring that surface form was removed [39]. Tactile horizontal resolution is dependent on the stylus tip radius which was 3 μm; vertical resolution was 12.8 nm. The vertical resolution on the Infinite Focus was set to 200 nm for shot peened surfaces and 100 nm for the ground surface in accordance with best practice recommendations [39]. Due to the relatively coarse shot peened surface profile with indent diameters of the order of tens of micrometres, a horizontal resolution of 3.5 μm was deemed sufficient for roughness analysis. All optical data was processed to remove spikes from the surface and fill holes with values interpolated from nearby data points; the reference plane was set appropriately.

Tactile data was taken from a minimum of 32 line profiles, eight on each of four samples. Optical data was taken from five area scans measuring 1.4 mm × 1.1 mm; line profiles were zig-zagged across the area to ensure sufficient profile length. For T0 the average R_a and S_a of the five small scans were checked against a larger scan (in which fewer repeat zig-zags were required) of dimension 3.9 mm × 1.1 mm and the error in both was found to be less than 2%. Thus data from five small scans was considered appropriate and allowed data to be collected from different surface locations to check coverage.

Calibration samples of known plastic strain were deformed using an electromechanical Instron 5569 using monotonic uniaxial tension (at low ε_p) in the same manner as was described in Section 2 and compression (at high ε_p) at extension rate 0.1 mm min^{-1} in accordance with ASTM E9 [40], using molybdenum disulphide as a lubricant to reduce barrelling effects. The changes in microstructure induced by compression are illustrated in Fig. 4. As the plastic strain increases, the grain structure changes with elongated pancake grains more evident. The prior austenite grains on the top surface appear to get larger as strain increases and become flatter on the front and side surfaces.

To obtain calibrated plastic strain profiles and hence (using the Ramberg–Osgood model) estimates of the variation in yield strength near the shot peened surface, microhardness testing, XRD profiles and EBSD area scans were performed on calibration samples and shot peened samples in the region near the peened surface (Fig. 5a). This approach requires the assumption that the cold work induced crystal deformation and dislocation formation resulting from shot peening affects crystallite size and strain (and associated misorientations) in the same way as monotonic uniaxial deformation; there will be some errors in this assumption associated with the cyclic behaviour of the present material. Given the relatively minimal cyclic softening reported in this material in Section 2, this error is not significant in the present material system when compared with the experimental errors in plasticity measurements (Section 4.3). In cases of more significant cyclic softening, it may be necessary to calibrate cold work based on cyclically stabilised uniaxial test samples. Process T0 (13A) is the industrially applied process and is thus the process for which the different plastic strain profiling techniques are compared. Once appropriate measurement techniques were established, the method was applied to compare the plastic strain profiles resulting from each peening process.

The method was also applied in determining how the dislocation profile within the samples changed after LCF; plastic strain data was obtained from the notched region of three T0 samples,

Table 4
Shot peening process parameters.

Process	Designation	Intensity	Coverage (%)	Shot diameter (mm)	Shot hardness (HRC)	Shot velocity (ms^{-1})
MI110R 04A 200%	T1	4A	200	0.28	45–52	26
MI230R 13A 200%	T0	13A	200	0.58	45–52	57
MI330R 13A 200%	T2	13A	200	0.84	45–52	35
MI330R 18A 200%	T3	18A	200	0.84	45–52	54

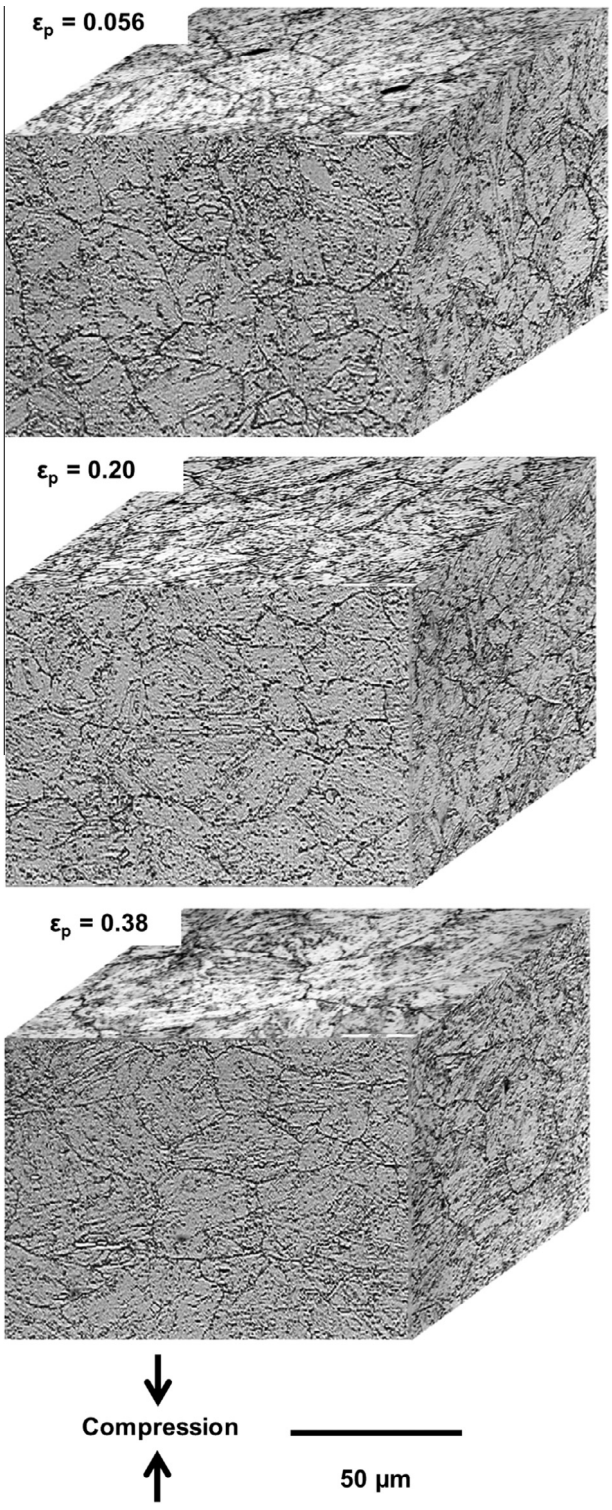

Fig. 4. Microstructure in calibration samples after compression to known plastic strains illustrating the development of elongated pancake grains.

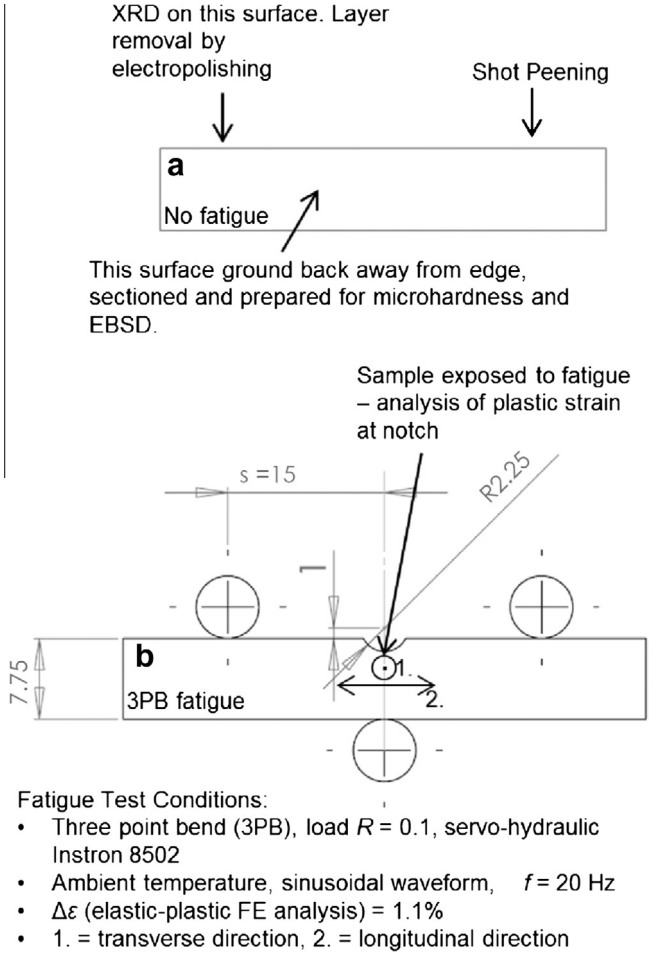

Fig. 5. Sample preparation.

one as peened, one after one fatigue cycle and one at half the fatigue life. The fatigue experimental details are detailed elsewhere [7] and are summarised in Fig. 5b. The strain at the notch root was calculated using elastic–plastic finite element analysis in Abaqus Standard. A quarter model was employed relying on specimen symmetry; the material model was based on the monotonic tensile test Ramberg–Osgood relationship and employed isotropic hardening to allow consideration of unloading behaviour. Elements were full integration 20 node quadratic hexahedral C3D20 type and were 0.01 mm in depth adjacent to the surface loaded in tension. A representation of the first loading cycle in terms of strain range (in the direction of the primary tensile axis) was obtained through sequential static analysis of stress and strain distributions under maximum and minimum load. The significance of the cyclic softening reported in Section 2 was investigated by changing the material model used; it was found that in terms of strain range the variation induced by using either the cyclically stabilised or combined material models was <2% and was less significant than the corresponding variation introduced by a 5% error in the applied load. Once it

had been verified that the plastic strain profile in the notch resulting from shot peening was representative of that on the flat section, parallels were drawn between the dislocation distribution, the cyclic softening behaviour and the residual stress relaxation behaviour in this specific material-loading system [7].

3.2. Microhardness

Microhardness profiles were obtained for each surface condition based on four traverses of indents separated by 10 μm on the polished face indicated in Fig. 5a. Testing was in accordance with BS EN ISO 6507-1:2005 [41] using 200 g load for 15 s dwell. An image analysis protocol was implemented to analyse the microhardness indents and their position with respect to the surface mean line. Data for multiple traverses were smoothed using a Loess function with a polynomial of degree 1 and sampling proportion of 0.3 to ensure any waviness in the data was removed.

3.3. XRD

The laboratory based XRD $\sin^2\psi$ method in combination with incremental layer removal by electropolishing (electrolyte = 8% (by volume) of 60% perchloric acid solution mixed in solution with 92% (by volume) of glacial acetic acid) was previously used on both flat and notched samples peened using process T0 to establish the compressive residual stress profile resulting from shot peening [7]: A Proto iXRD system with a Cr-Kα beam of wavelength 2.291 Å was used to make measurements on the {2 1 1} diffraction peak at a 2θ angle of approximately 156°. The accelerating voltage was 20 kV and the nominal current was 4 mA. A 0.5 mm collimator was used to reduce curvature effects in the notched samples since measurements were taken in both the loading (longitudinal) and the orthogonal (transverse) directions. Sample directionality is illustrated in Fig. 5b. When the beam was rotating in the axial direction (for measurements in the transverse direction), there were no notch shadowing effects and fourteen ψ angles were used in the range $-39 < \psi < 39°$ across two detectors. When the beam was rotating in the radial direction (for measurements in the longitudinal direction), notch shadowing was more significant and the fourteen ψ angles were in the range $-30 < \psi < 30°$. In the present work, the $\psi = 0°$ data was analysed to determine the line broadening depth profiles (defined by the FWHM of a Gaussian profile fit) that had occurred as a result of the shot peening process. In these conditions, the X-ray penetration depth in ferrite was estimated using data available in the literature [42] for Cr radiation on the {2 1 1} peak to be 5 μm.

Despite variations in the residual stress profile with measurement direction, there was no significant directionality found in the plastic strain profiles measured in the calibration or flat or notched T0 samples and as such the profiles were averaged. The error was approximated by calculating the sample standard deviation from 5 bi-directional measurements on the surface of the flat T0 sample; the resulting 95% confidence in FWHM measurements was ±0.12°.

3.4. EBSD

All cross sections for EBSD analysis were ground and polished to a 1 μm finish before final preparation using colloidal silica of 0.04 μm grain size. Data were collected using an EDAX Hikari EBSD camera operating at 300 fps used with a FEI Nova 600 Nanolab field emission gun scanning electron microscope operating at an accelerating voltage of 20 kV and a nominal current of 24 nA. Uncleaned data was processed in OIM vs. 5.2 and the patterns were indexed according to an α-iron structure.

All data was collected on an area measuring at least 200 × 200 μm using a step size of 0.4 μm (the shot peened samples were positioned with the edge such that with a scan size 200 × 250 μm, the sample area for collection was ~200 × 200 μm). This step size was validated by also collecting data at 0.2 μm for calibration samples and one T0 shot peened sample and comparing the analysed profile with those obtained at 0.4 μm. Two T0 samples were analysed at step size 0.4 μm, for each sample two different near surface areas were examined.

In the first instance, the same grain based method that was successfully applied in shot peened nickel based superalloy Udimet 720Li was used [8]. The results of this approach are illustrated in Fig. 6a. Although the colour coded map indicates that there is an increase in misorientation as measured by grain orientation spread (GOS) near the shot peened surface, the change in the smoothed data is too small to be able to confidently define the strain hardened region. This is a result of the high degree of intrinsic misorientation in this tempered martensitic material (revealed by underlaying the image quality parameter in greyscale in Fig. 6a) and as a result the application of a local misorientation method, kernel average misorientation (KAM) was investigated; the variation in the strain hardened region is illustrated in Fig. 6b.

This kernel approach resulted in many more data points than the original grain based approach. Data points with a KAM of 5° or greater were considered to represent block boundaries and removed since it was found that although the number of highly misoriented points increased near the peened surface, the analysis was less reproducible between analysis areas. The mean KAM at each depth (based on the sample surface mean line) was then calculated and the data were smoothed using the same procedure as for the hardness data. The strain hardened region can be clearly identified in Fig. 6b when the smoothed line is compared with the upper and lower unstrained bounds as identified from unstrained mean ±2 unstrained standard deviation.

4. Surface roughness and plastic strain results

4.1. Surface roughness

3D reconstructions of the surface topography for each sample surface condition are shown in Fig. 7a–e. Fig. 7f compares the line profile roughness parameters R_a and R_z with the areal equivalents S_a and S_z; there is no significant difference between optical and tactile line measurement techniques. It is clear that whilst the measurement of average amplitude parameters seems consistent when comparing areal and profile measurements, the areal measurement of maximum peak to valley height is significantly greater than the line measurement. This is indicative of the greater probability of finding a significant surface feature using areal scanning compared to line scanning.

4.2. Plastic strain measurements in compression samples

The results of the plastic strain indicators for the calibration samples are shown in Fig. 8. A power law least squares regression resulted in the most appropriate calibration curve for the percentage change in microhardness data shown in Fig. 8a; this is not surprising given the Ramberg–Osgood behaviour shown by FV448.

The 95% confidence bars are based on 20 measurements for each calibration sample; however there are clear issues with repeatability reflected by the large error bars and the low R^2 value. It was ensured that there was no variation in hardness with location on each sample to eliminate barrelling effects as the cause of this scatter. The resulting difficulty in quantifying the error in the calibration was one reason for the development of the other

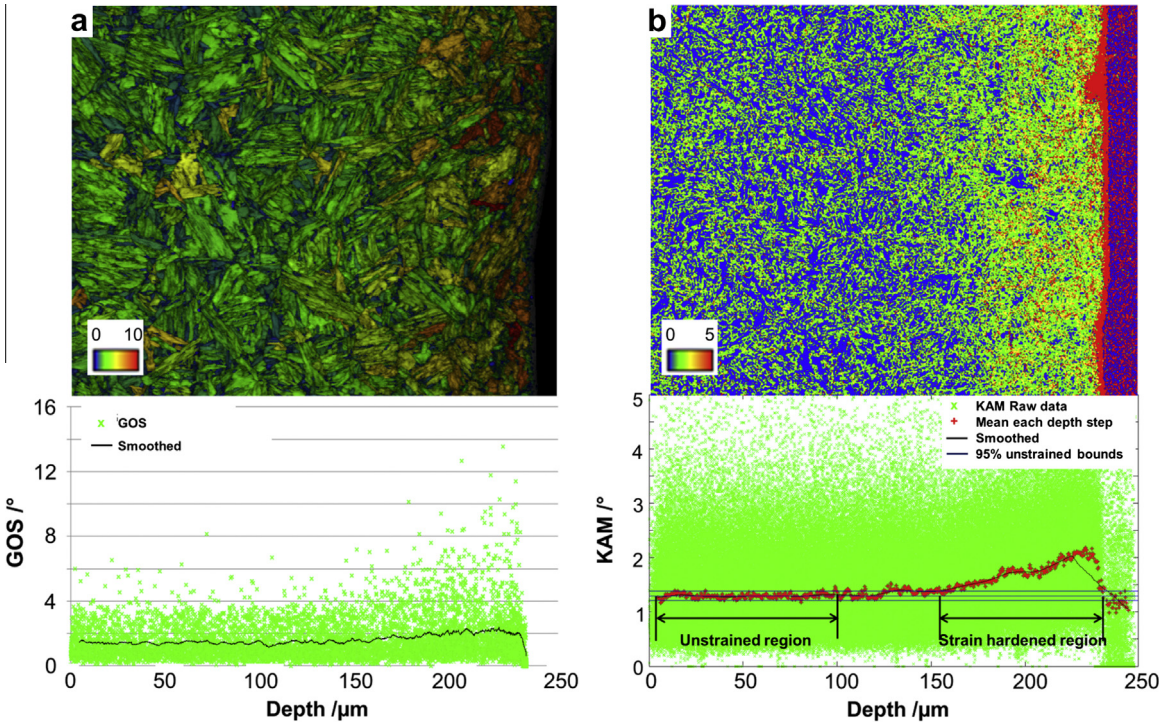

Fig. 6. Colour coded map indicating (a) grain orientation spread (with image quality in greyscale) and (b) kernel average misorientation for shot peening process T0 indicating the strain hardened region as identified by the local misorientation approach. (For interpretation of the references to colour in this figure legend, the reader is referred to the web version of this article.)

techniques as it meant that no error bounds could easily be placed on the calibrated data from shot peened samples.

Two least squares regressions were applied to the XRD FWHM data shown in Fig. 8b; both resulted in considerably higher R^2 values than the microhardness calibration. There was found to be no significant difference between the plastic strain profiles once they were applied. The power law (allowing a constant term for instrumental broadening) was selected rather than the exponential law (previously used by Prevéy [17,26] in nickel base alloys), since the fit was almost as good, was easier to apply as no numerical solution was required and allowed a more consistent comparison with the microhardness measurements. The error bars shown are constant at 0.12° as previously discussed and were not calculated for each measurement point; they are shown to indicate the order of the error existing in FWHM measurements on strained samples. Since this error is not well defined and R^2 was so high for this calibration, no error bounds were placed on the calibrated data from shot peened samples.

Using EBSD techniques, the KAM vs. plastic strain graph shown in Fig. 8c was determined for the calibration samples. There was no clear power law fit and so a straight line fit was applied. The EBSD data is more averaged than the other two approaches and the 95% confidence bars for each sample were based on 250,000 data points. The upper and lower bounds shown were calculated based on the average error across the 12 calibration samples; whilst the confidence in the fit is much better than for the microhardness data, it is lower than for the XRD data. This is exemplified by the mean points for two of the calibration samples lying outside the calibration error bounds. The high density data allowed account to be taken of this error. The unstrained KAM shown is known with a high degree of confidence, since it is the average of all the data points taken in the unstrained regions of the shot peened samples. Hence a linear shift was used to force the correct unstrained KAM in the calibration for each shot peened sample.

4.3. Plastic strain measurements in shot peened samples

Fig. 9 shows the repeatability of the EBSD measurement technique. The results of four scans on T0 samples at 0.4 μm step size are shown and compared with the result of the scan at 0.2 μm step size. The high level of repeatability in the data is clear and the profile of sample 1a was selected as representative of the T0 process. Applying the error bounds shown in Fig. 8 resulted in a far wider band than is required based on the data shown. Instead, in the present analysis all calibrated plastic strains were adjusted by 20%, this is equivalent to the worst case deviation from the mean line of the calibration sample at $\varepsilon_p = 0.2$ and resulted in the bounding curves shown in Fig. 9. The lower bound curve gives the lowest prediction of yield strength for a given misorientation and is considered representative for this data set; the lower bound is applied to all EBSD data presented in this paper from this point forwards.

The near surface plastic strain profiles after shot peening process T0 measured by the three techniques under consideration are compared in Fig. 10a. The corresponding yield strength profiles are compared in Fig. 10b. The XRD profile is very similar to the EBSD profile; despite the measurement of the surface plastic strain being higher using XRD, once calibrated to yield strength, the error at this point appears less significant as a result of the shape of the Ramberg–Osgood curve. Although at the first point of measurement, the yield strength determined by microhardness is not too dissimilar to that measured using the other two approaches, the profile extends much further into the sample. Indeed comparison with the residual stress data presented in Fig. 10c indicates that the plastic strain profiles measured using XRD and EBSD correlate very well with the depth of the maximum compressive residual stress at 150 μm; that measured using the hardness traverse extends to 250 μm which is closer to the overall depth of the compressive residual stresses at 340 μm.

The plastic strain profile resulting from each peening process as determined by EBSD is shown in Fig. 11. Measurements on ground

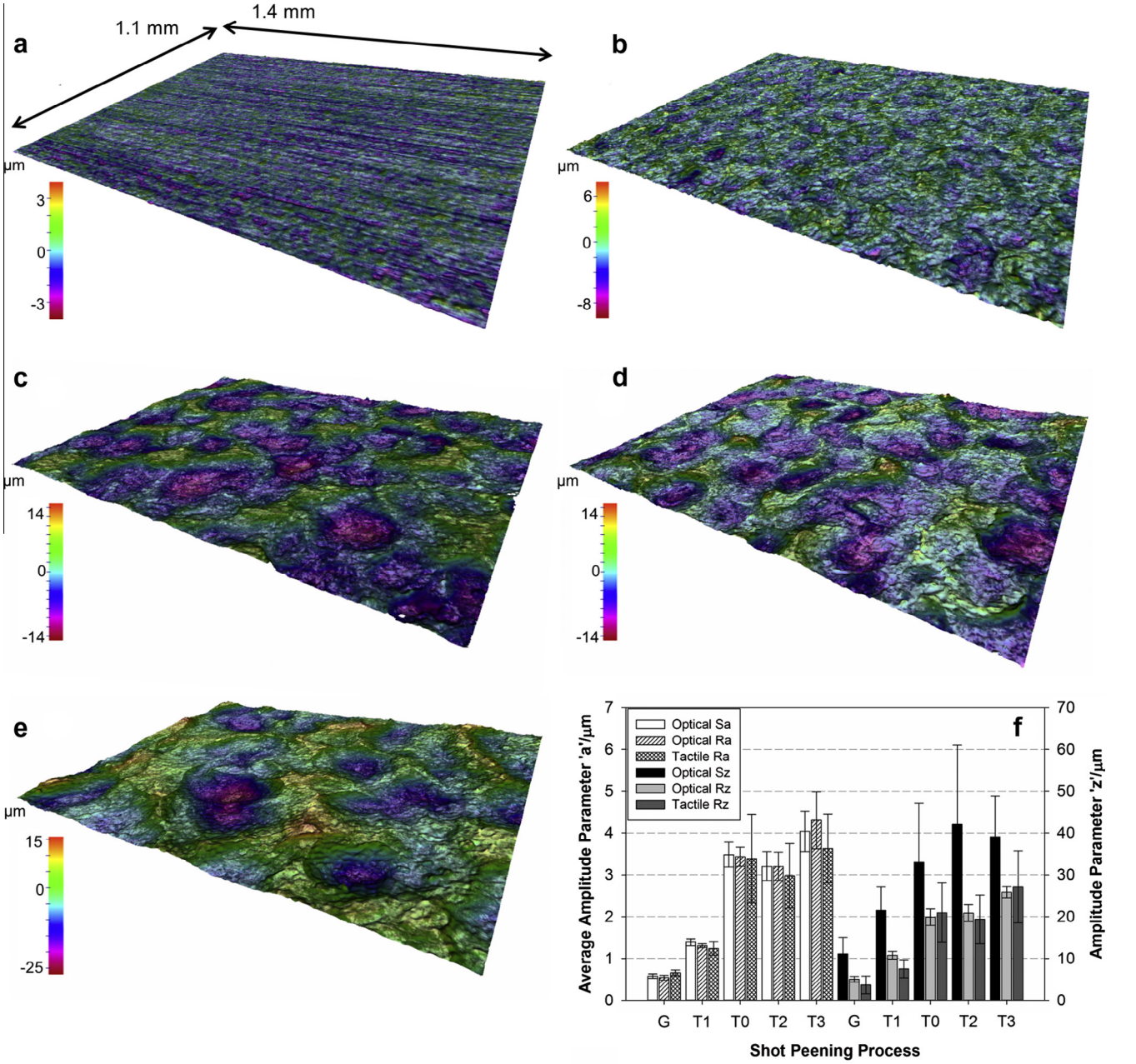

Fig. 7. 3D surface deformation generated by each surface preparation technique ((a) ground, (b) T1, (c) T0, (d) T2, (e) T3) and (f) comparison of surface roughness measurements for each surface condition.

samples did not detect any significant plastic strain profile. It is clear that the industrial 13A process (T0) resulted in the highest plastic strain in the near surface region. Increasing the intensity of the process to 18A (T3) resulted in a flatter profile near the surface but the same depth of profile, although the plastic strain remained high to a greater depth than in the industrial 13A process. Decreasing the intensity of the process to 4A (T1) resulted in a lower surface plastic strain and shallower profile. Increasing the shot size and reducing the velocity and maintaining the intensity at 13A (T2) resulted in a shallower profile with lower surface plastic strain compared to the industrial 13A (T0) process.

Changes in the near surface dislocation profile with fatigue exposure as determined by XRD are shown in Fig. 12. Comparison of the notched sample data before fatigue with that for the flat sample shown in Fig. 10a indicates that the notch geometry has had no significant effect on the induced plastic strain. The data after LCF suggests that after one cycle there is some rearrangement in dislocation distribution but that there are no further changes between this point and 50% of the total life.

5. Discussion

Greater areal maximum peak to valley measurements than line measurements have previously been reported for much rougher surfaces (R_a–20 µm) [43]. This trend is also present in the shot peened surfaces (R_a–3 µm) investigated in the present work. The implication for component lifing is clear: using the optical R_z data reported for T0 in the stress concentration assessment approach of Li et al. [10] and assuming that peaks are separated by the average indent diameter results in K_t = 1.25 (based on an average indent of 168 µm measured optically). Using the same empirical relationship

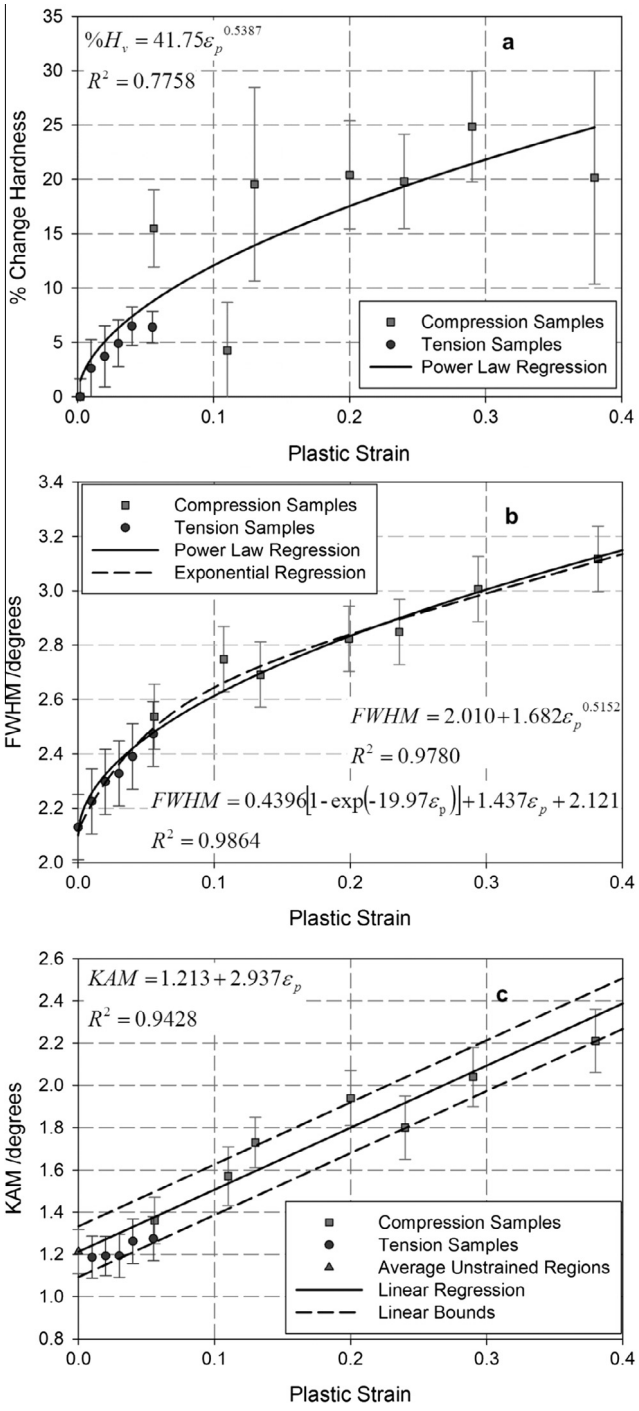

Fig. 8. Calibration equations for monotonic uniaxial tension and compression samples relating (a) % change in microhardness, (b) XRD FWHM and (c) EBSD KAM to plastic strain.

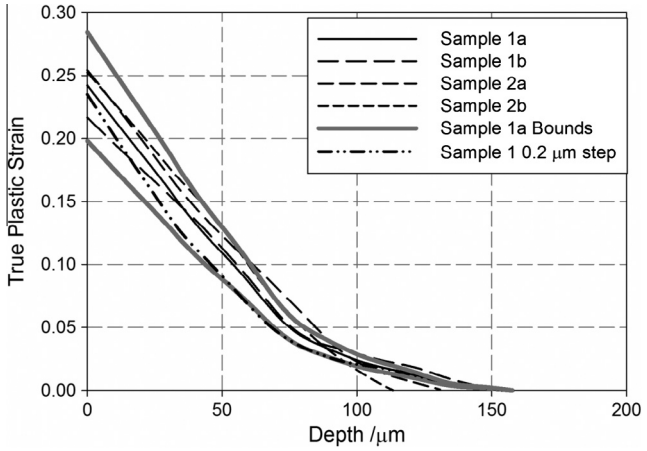

Fig. 9. EBSD profiles in T0 samples comparing 0.4 μm and 0.2 μm step size data and illustrating the lower bound consideration of error.

for S_z data results in $K_t = 1.42$, an increase of 13.6%. Despite the original paper [10] being based on finite element analyses and thus well-defined dent geometries, the approach is most typically applied using line profiles [44] which may not detect the worst case defect. The application of areal profiles increases the chance of picking up the worst case stress concentration and would represent a more conservative approach.

The accurate description of near surface strain hardening is important, especially if it is to be used in finite element models determining component stress and strain distributions for application in life assessment (for example following the procedure allowing variations in materials properties near the shot peened surface described by Benedetti et al. [45]). Furthermore, should near surface phase transformations be identified (there were none identified in the present system [7]), they should also be considered as a contributing factor to this material property gradient. Of the three approaches to measuring cumulative plastic strain presented in this paper, despite the difference in sample volume (XRD being greater than EBSD [28]), EBSD and XRD techniques are the most consistent. Although easy to use, there are several drawbacks to the microhardness technique, the first being that constraint effects prevent indents from being placed immediately next to the peened surface of interest. The other major drawback to the approach is the increase in indicated plastic strain depth resulting in a deeper elevated yield strength profile which could lead to non-conservative estimates of component remnant life. This might be a result of the influence of residual stresses on hardness measurements [19]. It is generally considered that plastic strain has the greatest influence on hardness, indeed interpolation based on the results of Xu and Li [46] indicates that in the present case, at the maximum residual stress $\sim -0.8\sigma^0$ and $E/\sigma^0 = 250$, the variation in hardness caused by residual stresses would be expected to be just 5%. However, given the sensitivity of the power law calibration at low plastic strains and the shape of the Ramberg–Osgood curve, even small changes in hardness could lead to increases in the estimated yield strength.

For this reason, the microhardness technique was not applied further in the present investigation. EBSD is advantageous over XRD in that many more data points are collected and results are more averaged, increasing confidence in the data. Since the XRD data is produced from discrete data points, the confidence in individual data points is lower. However, the calibration R^2 value was higher for XRD and although time consuming, FWHM data is typically available from the same data set as that used for residual stress measurements, so the approach could be applied if residual stress measurements were needed with no further data requirements. A key indication from the results in this paper is that a 'mix and match' approach can be used depending on which method is more appropriate to a given situation. Indeed we have done just that, applying the EBSD technique to compare the different peening processes where incremental layer removal XRD would have been too time consuming, and applying the XRD technique to investigate the effect of fatigue on dislocation distribution since the data was already available after residual stress analysis.

As expected, based on the work of Child et al. [8], peening at a higher intensity resulted in high plastic strains extending to a

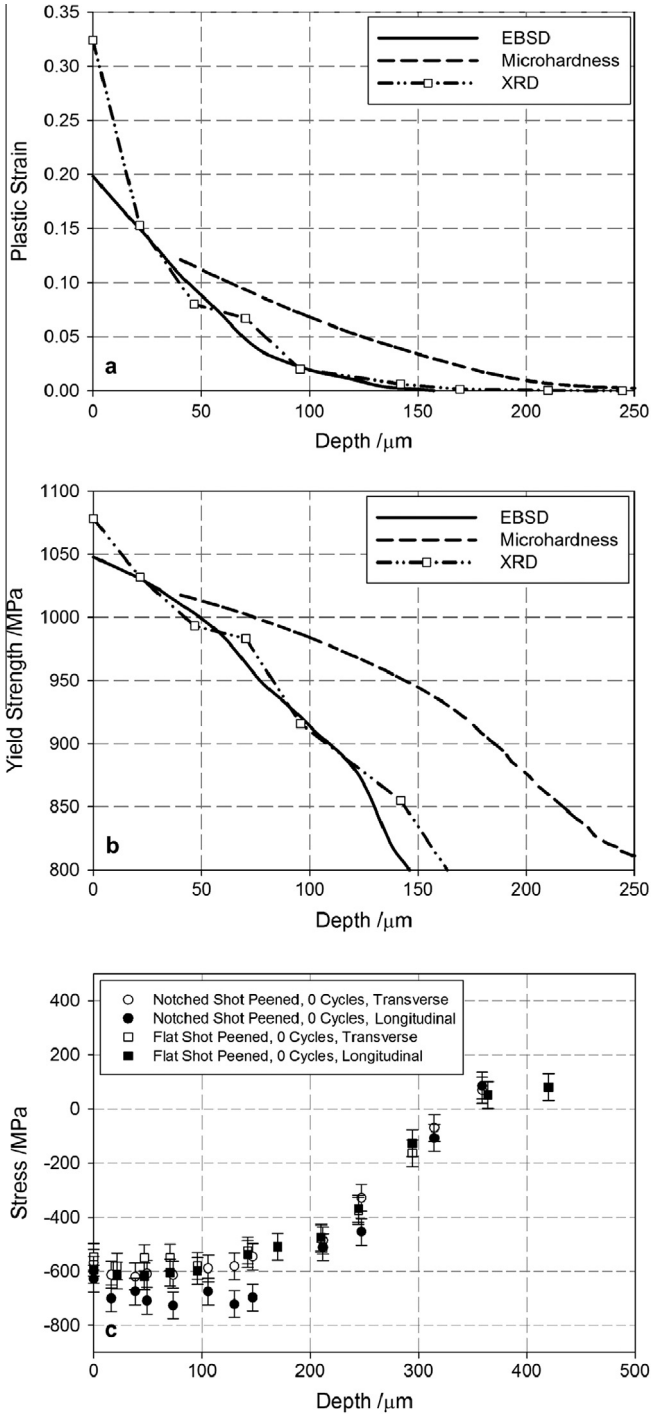

Fig. 10. Comparison of (a) plastic strain measured by the three different methods and (b) the corresponding yield strength distributions calculated using the Ramberg–Osgood relationship resulting from shot peening process T0; these results can be compared with (c) the residual stress profile measured using the XRD $\sin^2\psi$ technique (after Soady et al. [7]).

greater depth whilst peening at a lower intensity resulted in lower plastic strains and a shallower profile. However, the comparison of T0 and T2 is of interest in the present case. It is not just the intensity of the shot peening process which is important, but also the manner in which that intensity is achieved as this affects the resulting plastic strain profile. This new plastic strain data supports the previous conclusions based on residual stress measurements [18]. This emphasises the requirement for strain hardening and residual stress profiles for each target material – shot peening process system if the effects of the peening process are to be included in component lifing protocols. Furthermore, the need for a well optimised process is clear, despite the lower yield strength resulting from process T2 than T0, the worst case defect as measured by S_z is increased, indicating that the initiation life of samples peened using process T2 would be expected to be worse than those peened using T0.

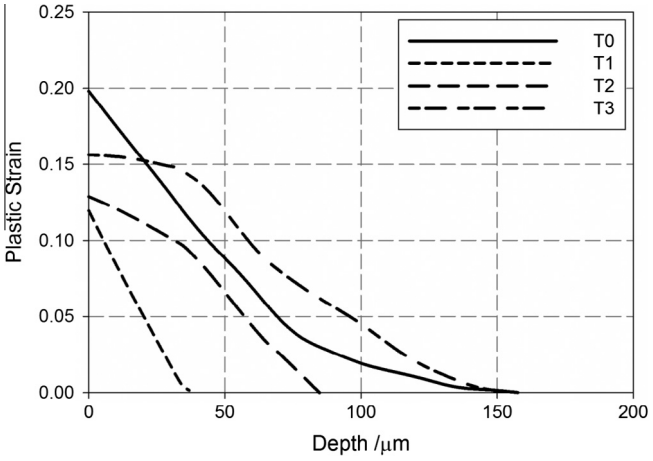

Fig. 11. Comparison of the plastic strain resulting from the four peening processes measured using the lower bound EBSD technique.

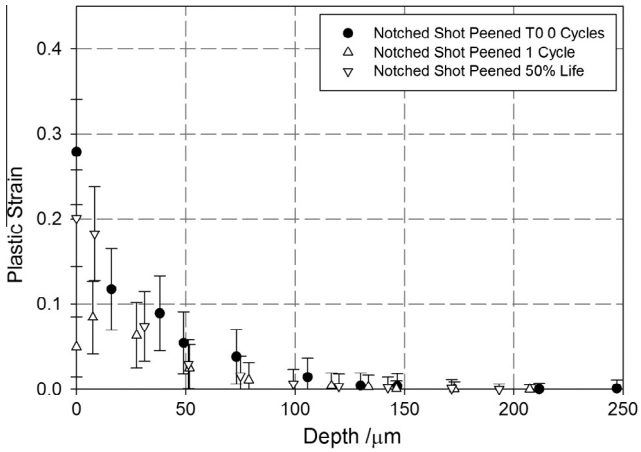

Fig. 12. Changes in the plastic strain profile with fatigue cycling at 1.1% notch root strain range measured using the XRD technique.

A note is made at this juncture of the significance of the materials models reported in Section 2. The combination of XRD residual stress measurement (reported in [7]), 3D surface topographical characterisation and plastic strain measurement by EBSD or XRD (reported in the present paper) results in sufficient data to implement the effects of the shot peening process in life assessment modelling of shot peened components. This could be implemented by incorporating the experimentally measured profiles in finite element models which determine local stresses and strains in a component (as recommended by Soady et al. [5]). This approach implicitly accounts for the effect of the type of work hardening in the material on the plastic deformation induced residual stresses at the start of life. However, the subsequent modelling of LCF should account for the effects of cyclic softening which may have occurred in the shot peened layer (for example by specifying the cyclically stabilised or combined material model such that the plasticity already experienced during peening is accounted for) and any changes in residual stress and plastic strain profiles observed during loading; these changes are discussed in the following paragraph for the present system.

The dislocation distribution after LCF was compared with the cyclic softening behaviour reported in Section 2. The cyclic softening in FV448 is associated with the sweeping of dislocations into a cellular structure; it is thought that it is this rearrangement of dislocations near the surface under the first cycle of load which results in the measured reduction in plastic strain. In FV448, the rate of softening reduces after the first load cycle; this explains the lack of continued logarithmic softening measured between the first cycle and 50% of life. This result can be compared with that of Dalaei et al. [11] in a pearlitic steel in which a logarithmic reduction in FWHM with fatigue cycling was reported and Kim et al.[12] in a Ni-base superalloy in which no change in FWHM profile was found at moderate temperatures; both other works employed a similar strain range to that under investigation here. Since these changes are dependent on the material cyclic stress–strain behaviour and the specific loading geometry, as previously mentioned, it is essential when considering the application of plastic strain and residual stress data in fatigue life assessments that any possible changes in the specific system are accounted for in the simulation.

The dislocation distribution after LCF was also compared with the residual stress relaxation results previously reported in the same sample [7]. It was found that the maximum compressive residual stress relaxed to 80% of the original value perpendicular to loading, but no relaxation was found in the direction parallel to loading after one cycle (this relaxation resulted from quasi-static stress relaxation mechanisms [47] and was associated with the highly constrained nature of three point bend loading) and no further changes were reported at 50% of the expected fatigue life. The lack of continued residual stress relaxation after one cycle correlates well with the lack of changes in dislocation distribution observed after the initial fatigue cycle.

Since there was no significant change in residual stress or strain hardening with LCF, it is thought that surface roughness is likely to have only a very small effect on fatigue behaviour in the present system where residual stresses and strain hardening will dominate. However, as previously mentioned, this will not always be the case and this should be a consideration of any analyst performing a remnant life assessment for a shot peened component.

6. Conclusions

- Microhardness, EBSD local misorientation and XRD FWHM measurements can all be used in conjunction with a series of calibration samples to calculate the yield strength profile resulting from shot peening. EBSD and XRD approaches showed the most consistent results with microhardness traverses tending to overestimate the extent of the strain hardened region. EBSD misorientation maps consist of more data points so the data is more averaged and the confidence is high, however, despite being more time consuming and only resulting in discrete data points, the XRD calibration R^2 value was higher than that of the EBSD method and the technique can be applied to data already collected for residual stress measurements.
- Increasing the intensity above an industrially optimised process may not necessarily increase the depth of the plastic strain profile but may result in higher plastic strains being retained deeper in the profile. Reducing the intensity of the shot peening process tends to reduce the magnitude and depth of the plastic strain profile. The plastic strain profile is not just dependent on intensity, but also on the combination of shot size and velocity.
- Changes in the plastic strain distribution during LCF can be correlated with material cyclic stress–strain characteristics, applied loading distributions and related to residual stress relaxation which occurs as a result of plastic deformation. In the current ferritic heat resistant steel investigated, FV448, under three point bend load conditions, the near surface plastic strain reduced slightly after one load cycle, in good agreement with the cyclic softening behaviour observed and previously observed residual stress relaxation characteristics.

Acknowledgements

Financial support from the Engineering and Physical Sciences Research Council, E.ON New Build and Technology Ltd. and The Royal Commission for the Exhibition of 1851 is gratefully acknowledged. Thanks are also extended to Jenny Crump, a student at the University of Southampton for her assistance in gathering microhardness data.

References

[1] Soady KA. Review: life assessment methodologies incorporating shot peening process effects; mechanistic consideration of residual stresses and strain hardening. Part 1: The effect of shot peening on fatigue resistance. Mater Sci Technol 2013;29:637–51.
[2] British Standard, BS EN 15305:2008 non-destructive testing – test method for residual stress analysis by X-ray diffraction; 2008.
[3] Grant PV, Lord JD, Whitehead PS. Measurement good practice guide no. 53: the measurement of residual stresses by the incremental hole drilling technique, NPL; 2002.
[4] Fontanari V, Frendo F, Bortolamedi T, Scardi P. Comparison of the hole drilling and X-ray diffraction methods for measuring the residual stresses in shot peened aluminium alloys. J Strain Anal 2005;40:199–209.
[5] Soady KA, Mellor BG, Reed PAS. Review: life assessment methodologies incorporating shot peening process effects; mechanistic consideration of residual stresses and strain hardening. Part 2: Approaches to fatigue lifing after shot peening. Mater Sci Technol 2013;29:652–64.
[6] Novovic D, Dewes RC, Aspinwall DK, Voice W, Bowen P. The effect of machined topography and integrity on fatigue life. Int J Mach Tool Manu 2004;44:125–34.
[7] Soady KA, Mellor BG, Shackleton J, Morris A, Reed PAS. The effect of shot peening on notched low cycle fatigue. Mater Sci Eng A 2011;528:8579–88.
[8] Child DJ, West GD, Thomson RC. Assessment of surface hardening effects from shot peening on a Ni-based alloy using electron backscatter diffraction techniques. Acta Mater 2011;59:4825–34.
[9] Koster W. Effect of residual stress on fatigue of structural alloys. In: 3rd International conference on practical application of residual stress technology, ASM, Indianapolis, IN, USA; 1991. p. 1–9.
[10] Li JK, Mei Y, Duo W, Renzhi W. An analysis of stress concentrations caused by shot peening and its application in predicting fatigue strength. Fat Fract Eng Mat Struct 1992;15:1271–9.
[11] Dalaei KK, Karlsson B, Svensson LE. Stability of shot peening induced residual stresses and their influence on fatigue lifetime. Mater Sci Eng A 2011;528:1008–15.
[12] Kim S-B, Evans A, Shackleton J, Bruno G, Preuss M, Withers PJ. Stress relaxation of shot peened Udimet 720Li under solely elevated-temperature exposure and under isothermal fatigue. Metall Mater Trans A 2005;36A:3041–53.
[13] Taylor D, Clancy OM. Fatigue performane of machined surfaces. Fat Fract Eng Mat Struct 1991;14:329–36.
[14] British Standard, BS EN ISO 25178-2:2012 geometrical product specifications (GPS) – surface texture: areal. Part 2: Terms, definitions and surface texture, parameters; 2012.
[15] British Standard, BS EN ISO 25178-6:2010 geometrtical product specifications (GPS) – surface texture: areal. Part 6: Classification of methods for measuring surface texture; 2010.
[16] Harada Y, Mori K. Effect of processing temperature on warm shot peening of spring steel. J Mater Process Tech 2005;162–163:498–503.
[17] Prevéy PS. The measurement of subsurface residual stress and cold work distributions in nickel base alloys. In: Young WB, editor. Residual stress in design, process and materials selection. Metals Park (OH): ASM; 1987. p. 11–9.
[18] Zinn W, Scholtes B. Influence of shot velocity and shot size on Almen intensity and residual stress depth distributions. In: Int Conf Shot Peening 9, International Scientific Committee on Shot Peening, Paris, France; 2005. p. 379–84.
[19] Tosha K. Characteristics of shot peened surfaces and surface layers. In: Asia-Pacific forum on precision surface finishing and deburring technology, Singapore; 2001. p. 193–201.
[20] Kamaya M. Characterization of microstructural damage due to low-cycle fatigue by EBSD observation. Mater Charact 2009;60:1454–62.
[21] Cahoon JR, Broughton WH, Kutzak AR. The determination of yield strength from hardness measurements. Metall Trans 1971;2:1979–86.
[22] Srikant G, Chollacoop N, Ramamurty U. Plastic strain distribution underneath a Vickers indenter: role of yield strength and work hardening exponent. Acta Mater 2006;54:5171–8.

[23] Balzar D. Voigt-function model in diffraction line-broadening analysis. In: Snyder RL, Bunge HJ, Fiala J, editors. Microstructure analysis from diffraction, international union of crystallography; 1999.
[24] Bruker AXS GmbH, DIFFRAC plus TOPAS 4.2 technical reference; 2009.
[25] Tan L, Ren X, Sridharan K, Allen TR. Effect of shot-peening on the oxidation of alloy 800H exposed to supercritical water and cyclic oxidation. Corros Sci 2008;50:2040–6.
[26] Prevéy PS. X-ray diffraction characterisation of residual stresses produced by shot peening. In: Niku-Lari A, editor. Shot peening theory and application. Gournay-Sur-Marne, France: IITT International; 1990. p. 81–93.
[27] Kamaya M, Wilkinson AJ, Titchmarsh JM. Measurement of plastic strain of polycrystalline material by electron backscatter diffraction. Nucl Eng Des 2005;235:713–25.
[28] Buchanan PJ, Randle V, Flewitt PEJ. A simple procedure for the assessment of plastic strain in electron backscatter diffraction patterns. Scripta Mater 1997;37:1511–8.
[29] Sáez-Maderuelo A, Castro L, de Diego G. Plastic strain characterisation in austenitic stainless steels and nickel alloys by electron backscatter diffraction. J Nucl Mater 2011;416:75–9.
[30] British Standard, BS EN 10002-1:2001 metallic materials – tensile testing – Part 1: Method of test at ambient temperature; 2001.
[31] British Standard, BS 7270:2006 metallic materials – constant amplitude strain controlled axial fatigue – method of test; 2006.
[32] Hales R, Holdsworth SR, O'Donnell MP, Perrin IJ, Skelton RP. A code of practice for the determination of cyclic stress-strain data. Mater High Temp 2002;19:165–85.
[33] Armas AF, Avalos M, Alvarez-Armas I, Peterson C, Schmitt R. Dynamic strain ageing evidences during low cycle fatigue deformation in ferritic–martensitic stainless steels. J Nucl Mater 1998;258–263:1204–8.
[34] Kim DW, Kim SS. Contribution of microstructure and slip system to cyclic softening of 9 wt.% Cr steel. Int J Fatigue 2012;36:24–9.
[35] Chaboche JL. A review of some plasticity and viscoplasticity constitutive theories. Int J Plasticity 2008;24:1642–93.
[36] Le-Guernic Y, Eckersley JS. Peenstress software selects shot peening parameters. In: Int conf shot peening 6, International Scientific Committee on Shot Peening, San Francisco, CA, USA; 1996. p. 481–92.
[37] British Standard, BS EN ISO 4287:2000 geometrical product specification (GPS) – surface texture: profile method – terms, definitions and surface texture, parameters; 2000.
[38] British Standard, BS ISO 4288:1998 geometric product specification (GPS) – surface texture: profile method: rules and procedures for the assessment of surface texture; 1998.
[39] Alicona, Alicona Infinite Focus IFM manual IFM 2.1.5. EN 16.06.2008; 2007.
[40] ASTM, ASTM E9-09. Standard test methods of compression testing of metallic materials at room temperature; 2009.
[41] British Standard, BS EN ISO 6507-1:2005 metallic materials – Vickers hardness test – Part 1: Test method; 2005.
[42] Fitzpatrick ME, Fry AT, Holdway P, Kandil FA, Shackleton J, Suominen L. Measurement good practice guide no. 52: determination of residual stresses by X-ray diffraction, NPL; 2005.
[43] Nwaogu UC, Tiedje NS, Hansen HN. A non-contact 3D method to characterize the surface roughness of castings. J Mater Process Tech 2013;213:59–68.
[44] Benedetti M, Bortolamedi T, Fontanari V, Frendo F. Bending fatigue behaviour of differently shot peened Al6082 T5 alloy. Int J Fatigue 2004;26:889–97.
[45] Benedetti M, Fontanari V, Santus C, Bandini M. Notch fatigue behaviour of shot peened high-strength aluminium alloys: experiments and predictions using a critical distance method. Int J Fatigue 2010;32:1600–11.
[46] Xu Z-H, Li X. Influence of equi-biaxial residual stress on unloading behaviour of nanoindentation. Acta Mater 2005;53:1913–9.
[47] Holzapfel H, Schulze V, Vöhringer O, Macherauch E. Residual stress relaxation in an AISI 4140 steel due to quasistatic and cyclic loading at higher temperatures. Mater Sci Eng A 1998;A248:9–18.